

THE NEAR INFRARED ABSORPTION

INNE INCEPT COMMITTE



THE NEAR INFRARED ABSORPTION SPECTRUM OF HYDROGEN TELLURIDE

By

JOHN JOSEPH SCHALLER

ABSTRACT

The problem was to obtain the rotational constants of hydrogen telluride from its near infrared absorption specturm.

The apparatus included the spectograph, the multiple traverse cell, and the chemical glassware. The spectrograph was a high resolution instrument designed for vacuum infrared aboseption measurements in the one to three micron region. It was calibrated by argon emission lines interpolated by Edser-Butler bands.

Hydrogen telluride was prepared by hydrolysis of aluminum telluride and stabilized by refrigeration of the absorption cell.

A rigid, symmetric top approximation was used to predict the rotational sub-bands. The selection rules for perpendicular bands and the intensities determined the band appearance.

The data was examined for P, Q, and R sub-bands; it is believed that only P and R branches were observed. The method of combination differences was used to determine the inverse moments of inertia, which were used to predict several lines. The predicted lines were compared with those observed and the rotational constants were compared with those determined from the far infrared.

THE NEAR INFRARED ABSORPTION SPECTRUM OF HYDROGEN TELLURIDE

Ву

JOHN JOSEPH SCHALLER

A THESIS

Submitted to the College of Science and Arts
Michigan State University of Agriculture and
Applied Science in partial fulfillment of
the requirements for the degree of

MASTER OF SCIENCE

Department of Physics and Astronomy

ACKNOWLEDGEMENT

I am grateful to Dr. T. H. Edwards for suggesting the problem and for his helpful advice in obtaining and analyzing the spectrum.

Dr. C. D. Hause graciously provided the use of the multiple traverse cell and allowed it to be modified. J. W. Boyd and W. E. Blass were also helpful.

TABLE OF CONTENTS

Chapter		
· I.	HYDROGEN TELLURIDE	1
	The Problem	1
	Limitations	. 1
II.	APPARATUS AND TECHNIQUE	3
	Instrumentation	3
	Calibration	5
	Multiple Traverse Cell	8
	Chemistry	11
III.	PREDICTED SPECTRA	14
	Symmetric Top Approximation	14
	Perpendicular Bands	16
	Intensities	17
	Symmetry Properties and Statistical Weights	18
	Type-A Bands	19
IV.	ANALYSIS OF DATA	21
	First Trials	21
	Combination Differences	23
	Computed Sub-bands	25
	Conclusions	3 5
RTRI.I	OCR APHY	36

LIST OF TABLES

Table		Page
I.	Argon Calibration	7
II.	Measured Spectrum Lines	9
III.	Trial Assignment Used in Determination of Rotational Constants	24
IV.	Rotational Constants for H2Te	26
٧.	Calculated Symmetric Top Perpendicular Band Lines and Intensities R-Branch	31
VI.	Calculated Symmetric Top Perpendicular Band Lines and Intensities P-Branch	32
VII.	Assignment of Observed Transitions and Comparison with Calculated Lines (First Lines of R-Branch)	34
	LIST OF FIGURES	
Figur	•	Page
Figure	Infrared Spectrograph	Page 4
1.		
1.	Infrared Spectrograph	4
1. 2.	Infrared Spectrograph	4
1. 2. 3.	Infrared Spectrograph	10 12
1. 2. 3.	Infrared Spectrograph	10 12 12
1. 2. 3. 4.	Infrared Spectrograph	10 12 12 15
1. 2. 3. 4. 5.	Infrared Spectrograph Refrigeration System Hydrogen Telluride Generator Gas Filling System H ₂ Te Model Normal Modes of H ₂ Te	10 12 12 15 15
1. 2. 3. 4. 5. 6.	Infrared Spectrograph Refrigeration System Hydrogen Telluride Generator Gas Filling System H ₂ Te Model Normal Modes of H ₂ Te H ₂ Te Spectrum	10 12 12 15 15 22
1. 2. 3. 4. 5. 6.	Infrared Spectrograph. Refrigeration System. Hydrogen Telluride Generator. Gas Filling System. H ₂ Te Model. Normal Modes of H ₂ Te. H ₂ Te Spectrum. Perpendicular Band P-Branch.	10 12 12 15 15 22 27

CHAPTER I

HYDROGEN TELLURIDE

The Problem

The problem was to determine the molecular constants of the hydrogen telluride molecule using high resolution infrared techniques. The approach was to make an analysis of the rotational sub-bands in the near-infrared absorption spectrum of the gaseous hydrogen telluride. The results of this analysis were the rotational constants or inverse moments of inertia used in the quantum mechanical model of the rotational energy levels. The rotational energy levels are in turn a fine structure on the vibrational energy.

Hydrogen telluride is the fourth member of the group including water, hydrogen sulfide, and hydrogen selenide. It is the least stable, but the most nearly symmetric, having the largest molecular weight of the group. Water and hydrogen sulfide have both been extensively studied (7). Neither hydrogen selenide nor hydrogen telluride have been studied so completely. Rossmann (6) has made an analysis of hydrogen telluride in the far infrared and obtained rotational constants. The near-infrared rotational structure had not been previously reported.

Limitations

This analysis covers only a very narrow region, the rotational subband of one vibrational mode in the vicinity of 4000 wavenumbers. However, no other strong absorption bands due to H₂Te were found between 1 and 2.7 microns. Only a relatively few lines on either side of the vibrational

frequency were well resolved. The analysis was limited to the assumption of a rigid symmetric top molecule. Thus, only transitions corresponding to the higher values of total angular momentum were assigned. Terms for centrifugal distortion and vibration-rotation interactions have been omitted from the analysis. These are small second order terms, neglected here, but should probably be considered in any more detailed study of the spectrum. No analysis has been made in terms of the asymmetry parameters which would be important for the transitions near the center of the band where the asymmetric nature of the molecule can no longer be neglected. Such an analysis should also be included in a more complete study.

The experimental part of this problem depended, to a large extent, upon the production and stabilization of the gaseous hydrogen telluride. This was expected to be a major problem at the outset and proved to be so. This problem, especially that of stabilization, was superimposed upon those usually associated with high resolution infrared spectroscopy. However, as it turned out, the gas was eventually stabilized to a sufficient extent to allow data to be obtained on several occasions.

The analytical part of this problem presented more subtle problems of interpretation of the data. Once the correct assignment was given to the transitions, the data would yield the rotational constants of the molecule, consistent with the data for this region. This was to be done under the assumptions and limitations listed above. The constants obtained would be compared with those already reported from the far infrared (6). The constants obtained would be an extension of information about the molecule to the near-infrared region.

CHAPTER II

A PPARATUS AND TECHNIQUE

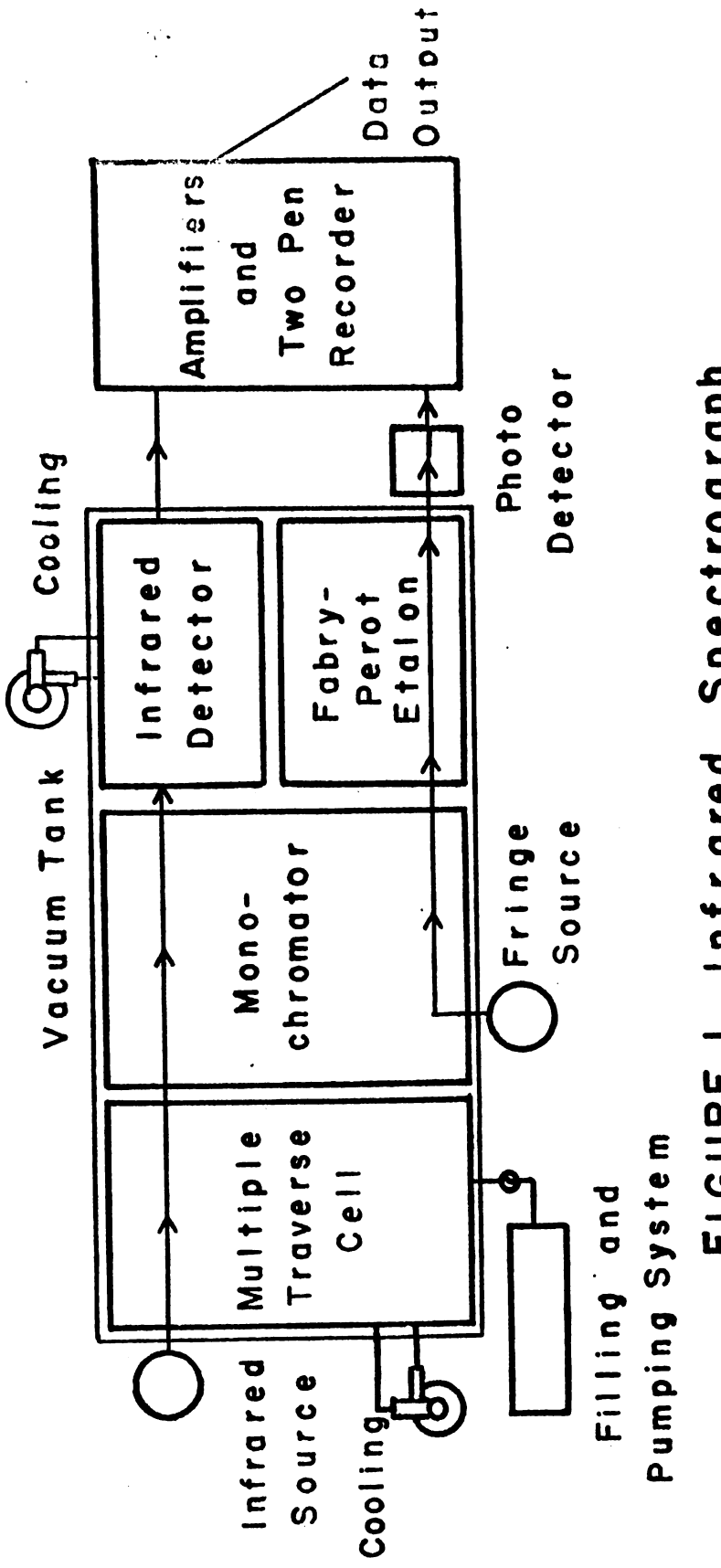
Instrumentation

The apparatus may be described in terms of three units. They are the spectrograph and its accessories, the multiple traverse cell, and the chemical glassware.

The apectrograph is a high resolution instrument designed for vacuum infrared absorption measurements in the one to three micron region. It is housed in a vacuum chamber containing the monochromator, foreoptics, and detector, and connected to a smaller chamber housing the multiple traverse cell and optics. The instrument is shown in schematic form in Figure 1.

The spectrometer uses a meflection grating in a Pfund type monochromator. The grating, a Bausch and Lomb certified-precision echelette, has 400 lines per mm and is blazed for the 3 micron region. The instrument was designed and built by Dr. R. H. Noble and has been modified by Dr. C. D. Hause and Dr. T. H. Edwards and their students.

The infrared detector was an Eastman Kodak lead sulfide cell cooled to -5% by a circulating mixture of dry ice and acetone. The signal goes to a cathode follower pre-amp and from there to a "lock-in" or phase sensitive amplifier and thence to a Leeds and Northrup two-pen recorder. The temperature variation of resistance of the detector was compensated by comparison of its resistance to that of a similar detector at the same temperature, but shielded from the infrared signal. The "dark" detector was used for this purpose as part of the resistance of the input circuit



Spectrograph FIGURE 1. Infrared

to the pre-amp. Cooling of the detector allows for a very good signal to noise ratio.

Calibration

Calibration was accomplished by interpolarion between argon emission lines appearing on the infrared record using Edser-Butler bands of constant wavenumber difference. These bands were obtained with a Fabry Perot etalon, an interferometer of fixed plate spacing. Bright fringes or maxima occur at wavelengths given by

$$\lambda = (2 \text{ d } \cos \theta)/m$$

where \(\) is the wavelength, d is the separation of the interferometer plates,

the angle of incidence, and m is any whole number (1). In this application, wis; ble light, which had taken essentially the same path through the monochromator as the infrared signal, illuminated the etalon at normal incidence. In wavenumbers, the relation becomes

$$\nu = m/2 d$$
, since $\theta = 0$ degrees.

As the grating was turned, decreasing wavelengths of light passed through the etalon producing a series of bright fringes. The fringe pattern is circular and appears to originate from (or terminate in) the center as the wavelength changes. Light from the center of this pattern was focused on a suitable photomultiplier. The photomultiplier signal was amplified and recorded by the two-pen recorder under the infrared record.

The wavelengths and wavenumbers of the argon lines were obtained from tables such as the M. I. T. wavelength tables (2,3). The fringes were numbered and the argon lines measured in terms of fringe number,

eta (a)

1

c. . . .

estimating to hundredths of a fringe. A linear curve of wavenumber against fringe number was plotted, with the form

$$\nu = Af + B$$

where # is the trial wavenumber, f is the fringe number, and A and B are respectively the slope and intercept of the curve.

Next, a plot of $(\gamma_0 - \gamma)$ was made, where γ_0 is the actual frequency (from tables) and a curve of the form

$$(1/2 - 1/2) = Df + E$$

was used to improve the first trial fit. This process was repeated until the weighted sum of the squares of the deviations was minimized.

Several of the argon lines, chosen for their intensity and narrow, symmetric shape, were given weights of two or three. An example of the data used in this fit is given in Table I. The final equation used for the calibration is

$$V = 0.401900 \text{ f} + 3901.928 \text{ cm}^{-1}$$
.

One of the important advantages of using interferometric calibration over mechanical means became evident when the spectra were examined for uniformity of the wavenumber--grating angle relation. This should have been a monotonically decreasing function with very small curvature. Over the extended range of the instrument this is the case, but for the small region of interest, a periodic shift of about 0.03 degreees in 0.42 degrees (4 cm⁻¹ in 50 cm⁻¹) was observed. This may be due to small periodic errors in the gear train, or to the selfsynchronous motor which turns the grating or perhaps the one which times the chart drive. This would be a limitation

TABLE I

ARGON CALIBRATION

Fringe Number	Observed Vo cm-1	Calculated of cm ⁻¹	Deviations Deviations Deviations
6.14	3904.347	3904.396	-0.049
82.74	3935.231	5.181	+0.050
250.90	4002.858	2.765	+0.093
289.90	4018.414	8.439	-0.025
319.09	4030.235	0.170	+0.065
508.50	4106.333	6.294	+0.039
559.89	4126.898	6.945	-0.047
950.25	4283.788	3.833	-0.045

of mechanical calibration, but since the fringes from the etalon provide a calibration independent of this problem, a linear fit was obtained with deviations less than 0.1 wavenumbers.

The spectra were measured against fixinge number and wavenumbers were assigned according to the calibration formula. In making both these measurements and those of the calibration, the average spacing of seven fringes around the desired line was used. This was done to cancel out small shifts in the fringe pattern. The lines and their assigned wavenumbers are given in Table II.

Multiple Traverse Cell

The multiple traverse cell, which holds the gas, is of the type designed by White (4). One of the important problems in obtaining good spectra was the rapid decomposition of the gas hydrogen telluride to its components. The tellurium deposited on all surfaces of the cell, especially the mirrors and windows (and on one occasion the whole sample leaked into and deposited on parts of the spectrometer). Since higher temperatures promote decomposition, the quartz windows of the cell, and the mirrors, at the image points, were the most heavily coated. To reduce this effect, it was decided to refrigerate the cell.

This was accomplished by wrapping the cell with copper tubing and circulating methanol as a coolant. The alcohol was cooled in a heat exchanger, giving up its heat to a mixture of dry ice and acetone, which was held in a large dewar. This system is shown in Figure 2.

TABLE II
OBSERVED SPECTRAL LINES

1 1 1 1 1 1 3990.591 0.70 4063.319 0.54 91.266 0.70 65.369 0.74 91.479 0.51 65.626 0.63 98.818 0.72 65.851 0.60 99.023 0.90 71.474 0.38 99.369 0.93 72.378 0.43 99.646 0.79 72.518 0.23 4006.217 0.80 73.431 0.08 6.426 0.73 75.605 0.40
91.266 0.70 65.369 0.74 91.479 0.51 65.626 0.63 98.818 0.72 65.851 0.60 99.023 0.90 71.474 0.38 99.369 0.93 72.378 0.43 99.646 0.79 72.518 0.23 4006.217 0.80 73.431 0.08
91.479 0.51 65.626 0.63 98.818 0.72 65.851 0.60 99.023 0.90 71.474 0.38 99.369 0.93 72.378 0.43 99.646 0.79 72.518 0.23 4006.217 0.80 73.431 0.08
98.818 0.72 65.851 0.60 99.023 0.90 71.474 0.38 99.369 0.93 72.378 0.43 99.646 0.79 72.518 0.23 4006.217 0.80 73.431 0.08
99.023 0.90 71.474 0.38 99.369 0.93 72.378 0.43 99.646 0.79 72.518 0.23 4006.217 0.80 73.431 0.08
99.369 0.93 72.378 0.43 99.646 0.79 72.518 0.23 4006.217 0.80 73.431 0.08
99.646 0.79 72.518 0.23 4006.217 0.80 73.431 0.08
4006.217 0.80 73.431 0.08
6.426 0.73 75.605 0.40
6.788 1.13 78.157 0.41
7.045 0.91 83.539 1.34
13.524 0.43 88.390 0.80
13.704 0.77 88.607 0.81
14.006 1.06 89.025 0.48
20.625 0.94 89.145 0.47
20.790 0.72 93.598 1.20
21.099 0.82 94.173 1.22
21.646 0.42 94.474 1.21
27.574 1.02 99.213 1.17
27.711 1.33 99.518 1.18
28.036 1.00 99.976 0.33
34 318 0.43 4104.072 1.22
34.527 0.60 4.550 1.50
34.792 0.61 4108.907 0.72
35.230 0.60 9.132 1.19
40.178 0.53 9.349 1.12
41.427 0.82 9.795 1.09
50.253 0.34 13.641 1.17
50.518 0.10 13.838 1.03 50.752 0.13 14.171 0.95
4057.857 0.33 18.061 0.86 58.086 0.40 19.464 0.52
59.324 1.00 22.294 0.70
59.513 1.00 22.732 0.84
59.762 0.90 23.648 0.65
62.869 0.40 23.853 0.58
63.082 0.57

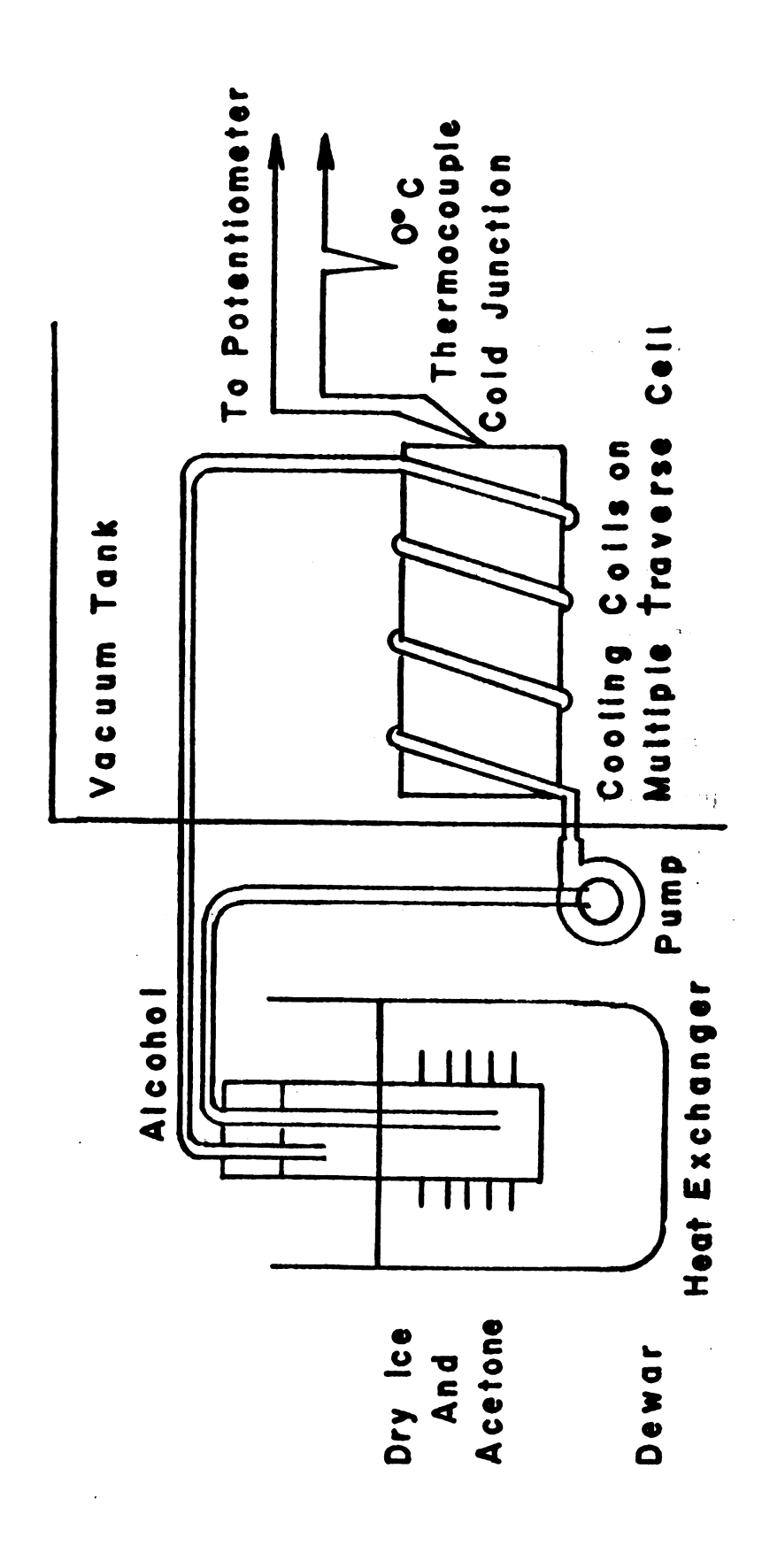


FIGURE 2. REFRIGERATION SYSTEM

Chemistry

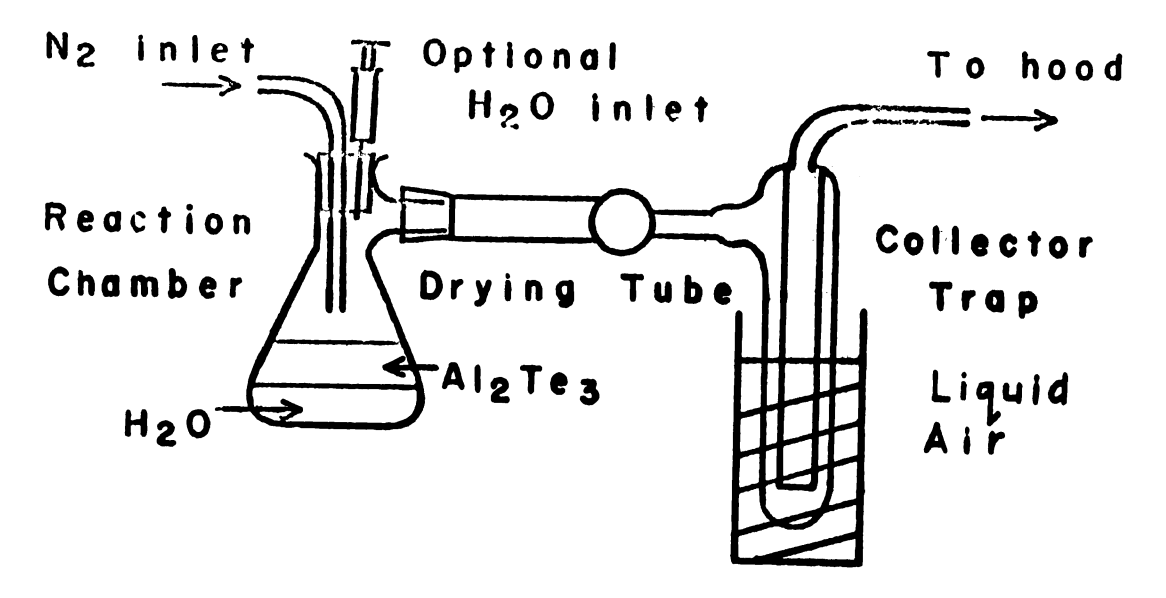
The hydrogen telluride was produced in small quantities immediately before each data run, since it decomposes readily upon standing, even at low temperature. It was produced by hydrolysis of aluminum telluride.

$$A1_2Te_3 + 6H_2O \rightarrow 3H_2Te + A1(OH)_3$$

The final form of the chemical glassware is shown in Figure 3. Hydrogen telluride is similar to hydrogen sulfide and hydrogen selenide in its chemical properties and may be handled by methods appropriate to those gases. The maximum allowable concentration in air for tellurium is given as 0.01 to 0.1 mg/cu meter (5).

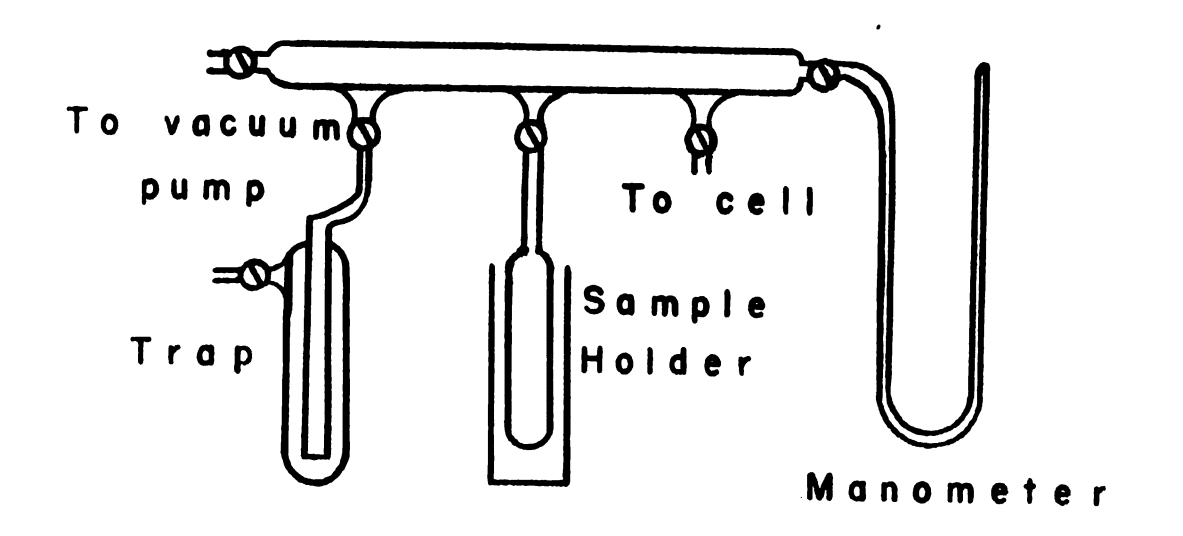
Decomposition of the gas occurs at room temperature in the presence of water, oxygen, organic substances, and light. In a large, uncooled version of the apparatus, hydrogen was the main product of the reaction and was burned as it left the system. The apparatus was much improved by simplication of the flow and by decreasing the size enough to allow cooling of the reaction chamber and the drying tubes. When cooled to nearly the ice point, the reaction was more efficient and usuable amounts of hydrogen telluride were produced.

Nitrogen served to sweep the system free of oxygen and hydrogen, and to carry the gas across, while water vapor was reduced by a simple trap charged with a convenient drying agent, such as calcium chloride, phosphorous pentoxide, or "Drierite." The hydrogen telluride was collected by freezing it out in a liquid air trap. Exit from the system was provided through wash bottles into a fume hood for any escaping gases.



Al₂Te₃ + 6H₂O \rightarrow 3H₂Te + Al(OH)₃ H₂Te $\stackrel{\triangle}{\longrightarrow}$ Te + H₂ \triangle : O₂, H₂O, heat, light

Hydrogen Telluride Generator FIGURE 3.



Gas Filling System FIGURE 4.

Water for the hydrolysis was put into the reaction chamber and frozen to about liquid air temperature. The aluminum telluride, in a finely powdered form, was then added, and the system closed and swept with nitrogen. Much heat was produced during the reaction, so the reaction chamber was cooled to below the ice point several times during the reaction by immersing it for a few seconds in liquid air.

The hydrogen telluride was stored in the trap at liquid air temperatures until ready for use. Just before being used, the gas was fractionally distilled into a gas sample holder as shown in Figure 4. This was done to remove any hydrogen formed and to further dry the gas before introduction into the cell. This was accomplished by carefully warming the trap, while keeping it below the ice point and collecting the distilled gas at liquid air temperatures in the sample holder. The gas could them be introduced into the cell by warming the sample holder while cooling the cell and could theoretically be recovered by the reverse process. In practice only small quantities were ever produced, and at the end of a run, nearly all of this had decomposed in the multiple traverse cell.

CHAPTER III

PREDICTED SPECTRA

Symmetric Top Approximation

In general, if a molecule has no three-fold or higher-fold axis, all three principal moments of inertia are different and the molecule is an asymmetric top. Hydrogen telluride, which belongs to the C_{2V} symmetry group, is an asymmetric top. Since the tellurium nucleus is so much heavier than those of the two hydrogens, the center of mass of the molecule is very close to the tellurium atom. Also, because the H-Te-H angle is so close to being a right angle, two of the principal moments should be nearly equal. To the extent that they are equal, H₂Te may be treated as an accidentally symmetric top.

For hydrogen telluride,

 $I_A = I_B = (1/2)I_C$, which would be the case for a plane symmetric rotor. Thus to a good first approximation, H_2 Te behaves like an oblate symmetric top. A model of H_2 Te is shown in Figure 5 where the principal axes are indicated. The molecule lies in the a-b plane, with c as the figure axis of the momental ellipsoid, but not of the moelcule. The normal modes of vibration are shown in Figure 6.

The rotational quantum levels are given by

$$F(J,K) = BJ(J+1) + (C-B)K^2 \qquad (equation 1)$$

where J is the quantum number of the total angular momentum, K is the component of J along the figure axis, and

^{*}c dxis

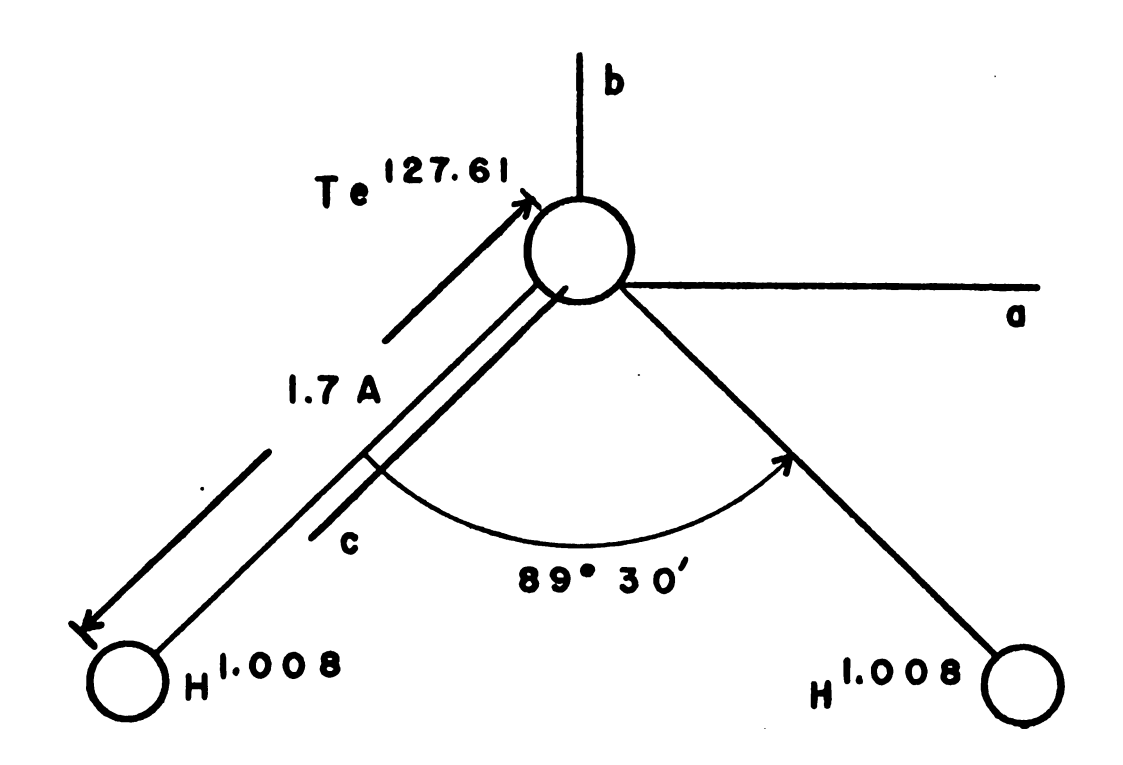
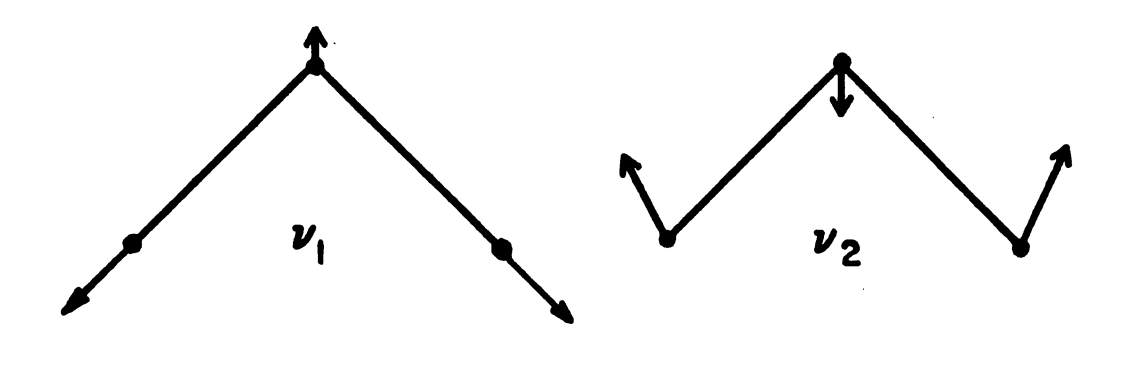


FIGURE 5. H₂Te Model



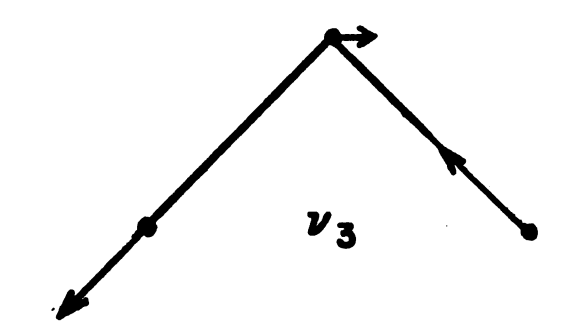


FIGURE 6. Normal Modes of H₂Te

 $|K| \le J$, that is K has eigenvalues K = J, J-1, ... -J.

B and C are the inverse moments of inertia, defined by $B = h/3\pi^2 c I_R \text{ and } C = h/8\pi^2 c I_C.$

where I_R and I_C are the principal moments of inertia,

h is Planck's constant,

c is the speed of light, and

 π is the numerical constant 3.14...

It should be noted that since C is now the unique molecular constant, this equation has a different appearance, but the same meaning as, for example, in Herzberg (7), equation (1,20), p. 24.

For the approximate value of B, an average has been used,

$$\bar{B} = 1/2(A + B) .$$

Perpendicular Bands

The appearance of the sub-bands is determined by the allowed transitions or selection rules and by the intensity of the lines. For a trial commic molecule, such as H₂Te, only perpendicular bands can occur. The selection rules that apply are

$$\triangle K = {}^{+}1, \qquad \triangle J = 0, {}^{+}1.$$

The sub-band for a given transition is designated by the notation of Herzberg (7) that a change of +1, 0, or -1 is labeled R, Q, or P respectively and the value of ΔK , ΔJ , and K and J for the initial state are put into the form $\Delta K_{K}(J)$. $R_{Q_{K}(J)}$ implies $\Delta K = +1$, $\Delta J = 0$, K'' = K, K' = K + 1; J'' = J' = J. Since $J \geq K$, lines for which J < K are "missing."

antes t

The frequencies of lines in the sub-bands are obtained by taking the difference between rotational levels:

$$V_{J''K''}^{J''K'} = V_0 + F'(J',K') - F''(J'',K''),$$

where ν_0 = G' - G" for the vibrational energy; the vibrational energy ν_0 corresponds to the summation band ν_1 + ν_3 of μ_2 Te.

For example,

$${}^{R}R_{K}(J) = V_{O} + (C' + B') + 2(C' - B')K$$

$$+ ((C' - B') - (C'' - B''))K^{2}$$

$$+ (3B' - B'')J + (B' - B'')J^{2}$$
(2)

$${}^{\mathbf{P}}\mathbf{P}_{\mathbf{K}}(\mathbf{J}) = \mathbf{V}_{\mathbf{0}} + (\mathbf{C}' - \mathbf{B}') - 2(\mathbf{C}' - \mathbf{B}')\mathbf{K}$$

$$+ ((\mathbf{C}' - \mathbf{B}') - (\mathbf{C}'' - \mathbf{B}''))\mathbf{K}^{2}$$

$$- (\mathbf{B}' + \mathbf{B}'')\mathbf{J} + (\mathbf{B}' - \mathbf{B}'')\mathbf{J}^{2}$$
(3)

The first lines of these sub-bands are obtained by setting J = K,

$${}^{R}R_{K}(K) = V_{o} + (C' + B') + (2C' + (B' - B''))K + (C' - C'')K^{2}$$
(4)

$${}^{\mathbf{P}}\mathbf{P}_{\mathbf{K}}(\mathbf{K}) = \mathbf{V}_{\mathbf{o}} + (\mathbf{C}' - \mathbf{B}') - (2\mathbf{C}' - (\mathbf{B}' - \mathbf{B}'')) \mathbf{K} + (\mathbf{C}' - \mathbf{C}'')\mathbf{K}^{2}.$$
 (5)

Intensities

The intensity of a line depends upon the statistical weight of the levels and upon the "expectation" that the transition will occur. The population of the energy levels depends upon the thermal distribution

$$N_{J,K} \propto g_{J,K} \exp -(E(J,K)/kT).$$

The line intensity is given (7) by the expression

$$I(J,K) = C A_{JK} g_{J,K} \exp -F(K,J) hc/kT$$
 (6)

where C is approximately a constant for a given vibrational transition,

 $\mathbf{g}_{\mathbf{J},\mathbf{K}}$ is the statistical weight,

F(J,K) the term value for the lower state and

 A KJ is proportional to the square of the transition moment summed over all values of M. For perpendicular bands, the $A_{\nu_{T}}$ are:

For
$$\Delta J = +1$$
: $A_{KJ} = \frac{(J + 2^{\frac{1}{2}} K) (J + 1^{\frac{1}{2}} K)}{(J + 1) (2J + 1)}$, (7)

$$\Delta J = 0: A_{KJ} = \frac{(J + 1 \pm K) (J + K)}{J(J + 1)},$$
 (8)

$$\Delta_{J} = -1$$
: $A_{KJ} = \frac{(J - 1 + K) (J + K)}{J(2J + 1)}$, (9)

where the upper sign refers to $\Delta K = +1$, the lower sign to $\Delta K = -1$ and J refers to the lower state. For K = 0, $\Delta K = +1$, the value must be multiplied by 2.

For the case of a symmetric top, the interaction between rotation and vibration may cause the structure of the Q branches to change. The difference between C', B' and C", B" causes the individual lines of a Q branch to no longer exactly coincide, and the series of Q branches converge slightly.

Symmetry Properties and Statistical Weights

Molecules with one pair of identical nuclei, such as $\rm H_2O$ or $\rm H_2Te$, have the symmetry of the point group $\rm C_{2v}$. Since the two-fold axis coincides with the b-axis, the axis of intermediate moment of inertia, the levels

that are positive or negative with respect to C_2^b are symmetric or antisymmetric respectively. (Rotational levels are positive if the total eigenfunction remains unchanged in sign for an inversion.) The behavior with respect to C_2^b is the product of the operations C_2^c and C_2^a ; that is, symmetric levels are ++, -- and antisymmetric are +-, -+ with respect to C_2^c and C_2^a . (The highest level J_{+J} for each set of a given J is + with respect to C_2^c , the next two down are -, and so on, while the lowest level J_{-J} is + with respect to C_2^a , the two next higher are -, and so on.)

These considerations result in a selection rule in addition to the change of one for J. "If the dipole moment lies in the axis of intermediate moment of inertia (b-axis), only the transitions

can take place." (7)

The statistical weights of the symmetric and antisymmetric levels depend upon the spin of the identical nuclei. For molecules with identical nuclei having non-zero spin the s and a levels are both present with different statistical weights. In particular, for a molecule such as H₂O or H₂Te, the antisymmetric on -rotation at times the statistical weight of the symmetric levels. (The nuclear spin of hydrogen is taken as 1/2.) There are thus two modifications of H₂Te, on the and para.

Type-A Bands

For a molecule in the point group C₂v, there are three types of infrared band, depending on the direction of the change of dipole moment. The types

÷ :

are designated A, B, or C for a change of dipole moment in the direction of the axis of least, intermediate, or largest moment of inertia, respectively (7).

The structure depends on the relative values of the moments of inertia. An important parameter is the ratio of the two smaller moments of inertia $(p = B/A = I_A/I_B)$ of a plane molecule for which $I_A + I_B = I_C$. For the limiting case p = 1, $I_C = 2I_A$ and C = (1/2A). This is approximately true for H_2 Te. The band structure is then similar to that of the perpendicular band of the symmetric top. The Q branch separation is 2C, while that of the P and R branches is 4C; the resulting series of lines would have a spacing of 2C. This is subject to the approximation that the constants for the upper and lower states are the same, that is, A' = A'', B' = B'', and C' = C''. The three branches will be shaded one direction at the other if this approximation does not hold. If the rotational constants are very different, the lines may not crowd in the center of the band; and the band may not show a Q branch.

The doublet lines corresponding to the two highest J values, J_{+J} , J_{+J-1} levels in the R and P branches have a spacing of approximately 2A, while for the lowest levels J_{-J} , and J_{-J+1} the spacing would be approximately 2C. These doublets should be fairly prominent.

There is an intensity alternation due to the presence of identical nuclei. The intensity ratio of lines connecting levels in the orthomodification to those in the para- is the ratio of their statistical weights, that is , 1:3 for H₂Te.

CHAPTER IV

ANALYSIS OF DATA

In order to make an analysis of the spectrum, shown in Figure 7, it was necessary to find approximate values of the rotational constants C', C", B', B" and V_o. This was done by examining the line spacing and attempting to obtain a rough fit on the basis of the oblate symmetric top approximation. A trial assignment of transitions was made to several of the lines on the basis of spacing and intensity. The constants were then determined by the method of combination sums and differences. The constants thus obtained were then used in the expressions for the sub-bands and the resulting calculated spectral lines were compared with the observed lines and additional transitions assigned where possible.

First Trials

The first trials used the rotational constants found by Rossmann (6) in an attempt to locate the P, Q and R branches. However, these values were derived from data in a different region and were for a different upper state. As a result, no agreement between observed and calculated lines was found for this first trial.

No series of lines were found which could be satisfactorily assigned to Q branches. The assumption was made that the Q branches were spread out and of low intensity. This could occur if the difference between the values of the rotational constants B', C' and B", C" in the upper and lower states was large enough.

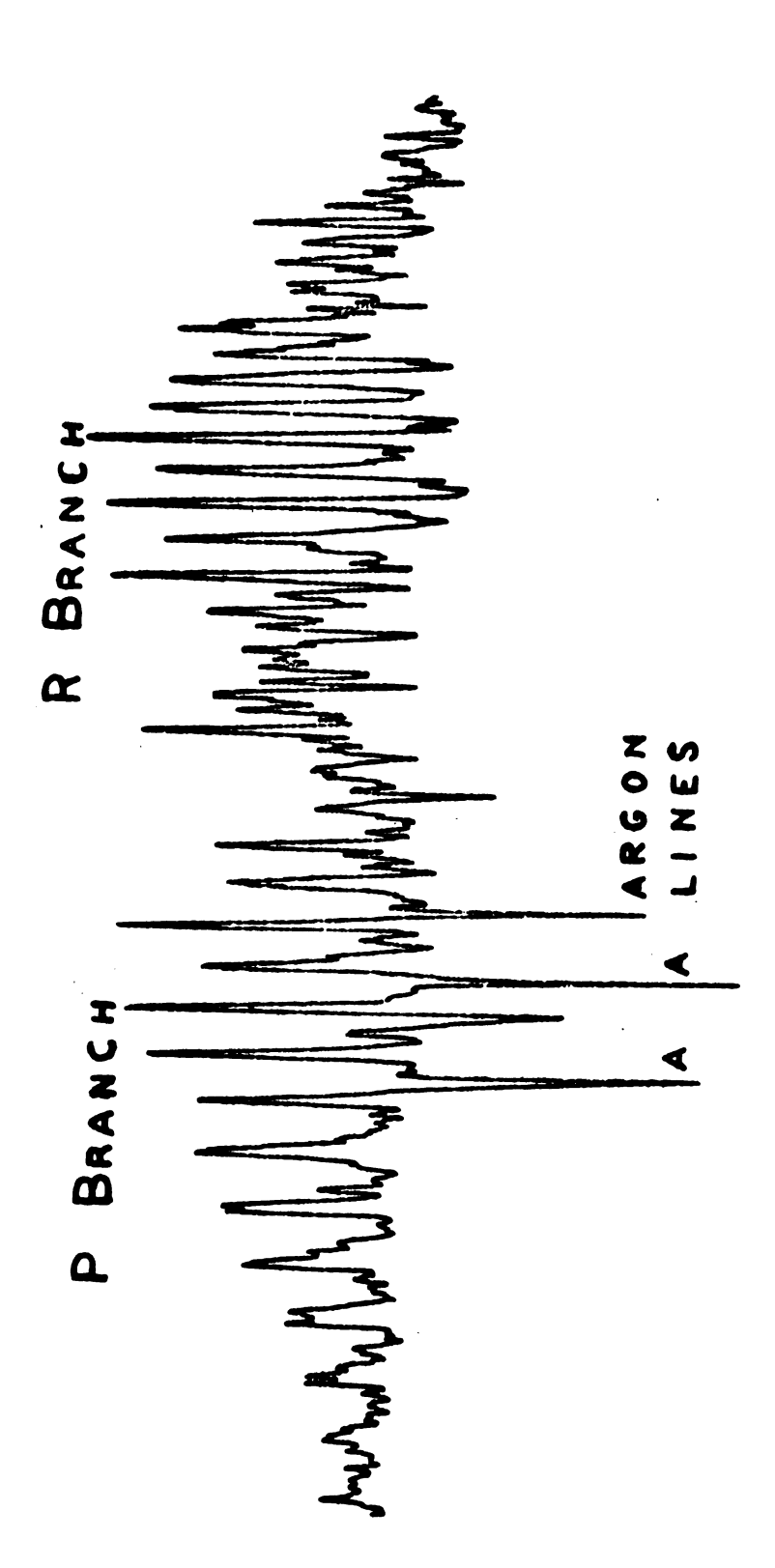


FIG. 7 H2TE SPECTRUM

Next an attempt was made to assign the lines to ${}^{\mathbf{P}}\mathbf{P}$ and ${}^{\mathbf{R}}\mathbf{R}$ branches. A trial assignment was made of transitions of the type ${}^{\mathbf{R}}\mathbf{R}_{\mathbf{K}}(\mathbf{K}+1)$ and ${}^{\mathbf{P}}\mathbf{P}_{\mathbf{K}}(\mathbf{K}+1)$ to a series of lines. The lines chosen and their assignments are given in Table III. The rotational constants were determined from these lines by the method of combination sums and differences.

Combination Differences

Simpler relations are obtained among the constants by the use of combination sums and differences. The transitions ${}^RR_K(J+1)$, ${}^PP_K(J+1)$, and ${}^PP_{K+2}(J+3)$ evaluated for J=K are given by:

$${}^{R}R_{K}(K+1) = \nu_{o} + C' + 5B' - 2B'' + (2C' + 3(B' - B''))K + (C' - C'')K^{2}$$

$${}^{P}P_{K}(K+1) = \nu_{o} + C' - B' - 2B'' + (2C' - 3(B' - B''))K + (C' - C'') K^{2}$$
(10)

and

$${}^{P}P_{K+2}(K+3) = V_{o} + C' - 4C'' + 5B' - 8B'' + (2C' - 4C'' + 3(B' - B''))K + (C' - C'')K^{2}$$
(12)

Forming sums and differences between these transitions gives:

$${}^{R}R_{K}(K+1) - {}^{P}P_{K}(K+1) = 6B' + 4C'K$$
 (13)

$${}^{R}R_{K}(K+1) + {}^{P}P_{K}(K+1) = 2\gamma_{o} + 2C' + 4(B' + B'') + 6(B' - B'')K + 2(C' - C'')K^{2}$$
(14)

TABLE III

TRIAL ASSIGNMENT USED IN

DETERMINATION OF ROTATIONAL CONSTANTS

к —	$\frac{R_{\mathbf{K}}(\mathbf{K}+1)}{\mathbf{cm}^{-1}}$	P _K (K + 1)
1		4041.43
2		3 ⁴ ·79
3	4099.72	28.04
4	104.55	21.10
5	109.13	14.01
6	113.64	6.79
7	118.06	3999 - 37
8	122.29	
9	126.30	
10	130.23	

$${}^{R}R_{K}(K+1) - {}^{P}P_{k+2}(K+3) = 6B'' + 4C'' + 4C''K$$
 (15)

$${}^{R}R_{K}(K+1) + {}^{P}P_{K+2}(K+3) = 2 V_{o} + 2C' + 10(B' - B'')$$

$$-4C'' + (4(C' - C'') + 6(B' - B''))K + 2(C' - C'')K^{2}$$
(16)

These equations (12, 13, 14, 15) may be used to determine the constants B', B'', C' and C'', and $V_{C'}$.

Plots of equations (12) and (14) were both linear; B' and C' were determined by (12) and B" and C" by (14). Equations (13) and (15) have quadratic terms with the coefficient 2(C' - C''). The intercepts of these equations include the term γ_0 which may be determined in this way. The rotational constants obtained from this analysis are given in Table IV. Computed Sub-bands

Using these rotational constants in equations (2) and (3), sub-bands were computed for K values up to 15 and J values up to 24. These computations were carried out on the Michigan State high speed computer MISTIC. Calculated lines for values of K and J up to eleven were plotted with their calculated intensities and compared with the observed spectral lines. The ^{P}P branch lines are shown in Figures 8 and 9, while the ^{R}R branch lines are shown in Figures 10 and 11. The calculated R-branch lines together with their relative intensities are given in Table V for the first lines of the sub-bands (J = K) up to K = 15. The second and third lines are given in Table VI.

A number of the observed lines were assigned to transitions of the type $^RR_K(K)$ and $^PP_K(K)$ and compared with the calculated lines. These are given

TABLE IV

ROTATIONAL CONSTANTS FOR \mathbf{H}_2 Te

C' = 2.935 cm⁻¹

C'' = 3.006

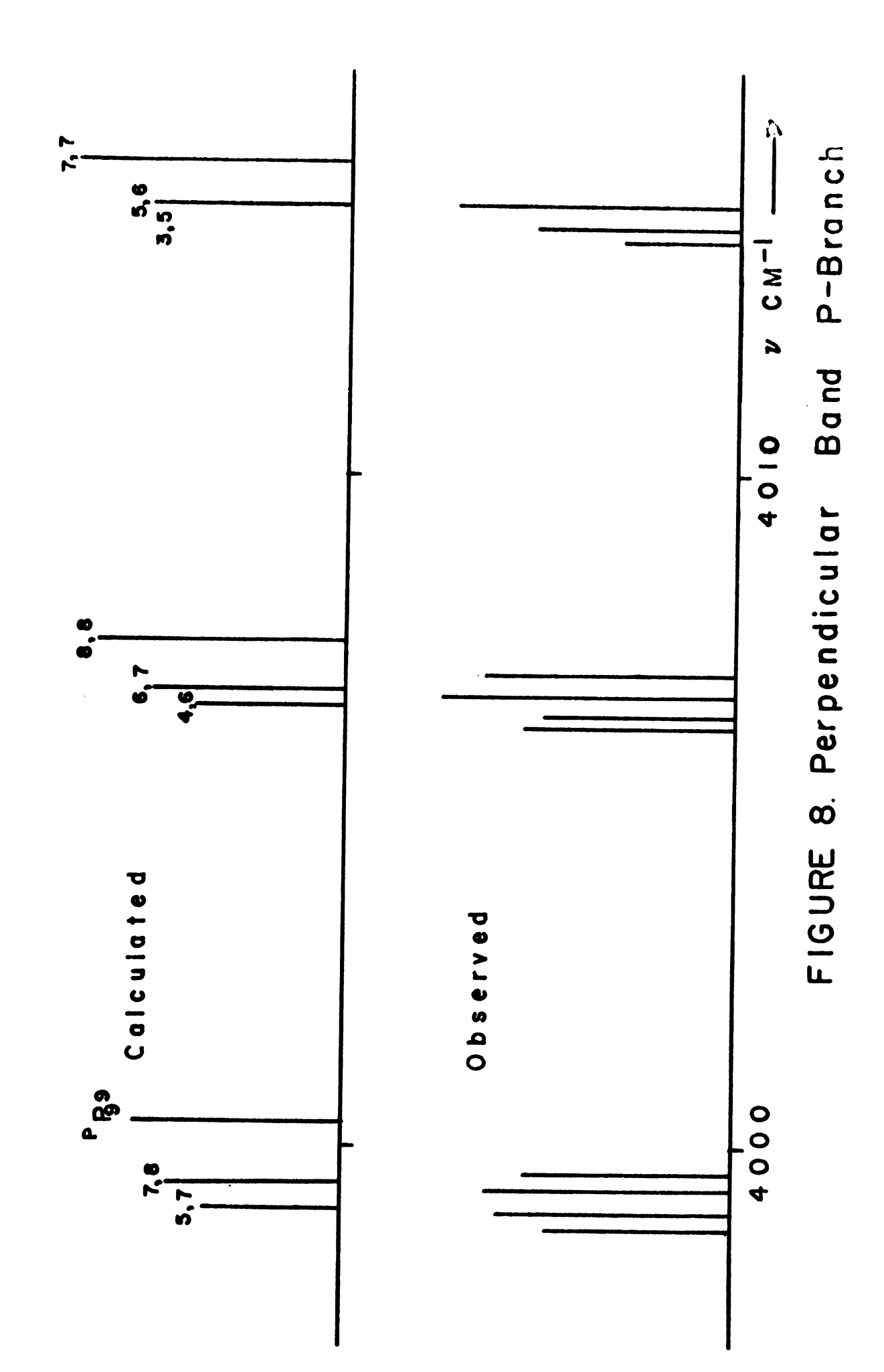
B' = 6.075

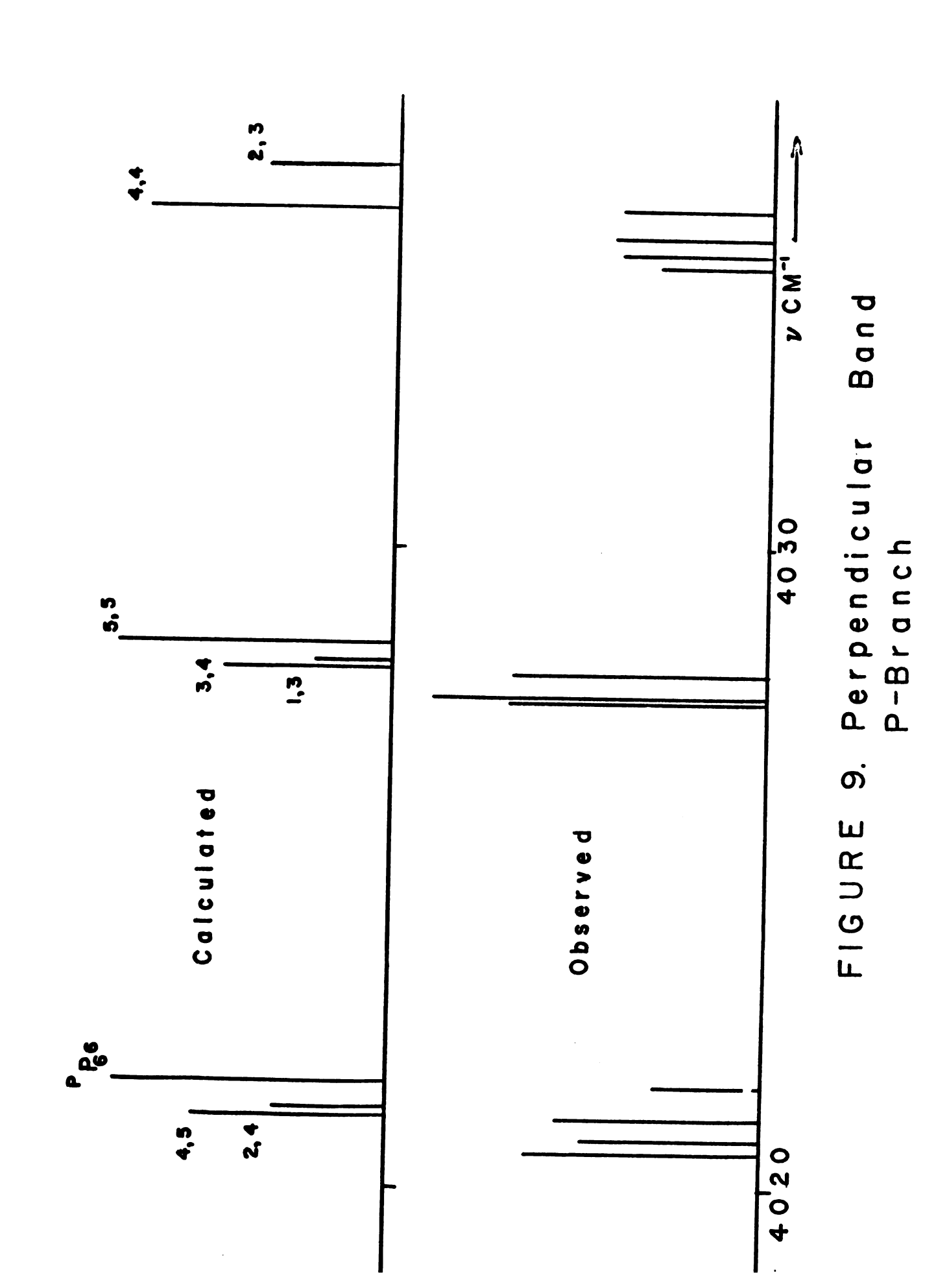
B'' = 6.270

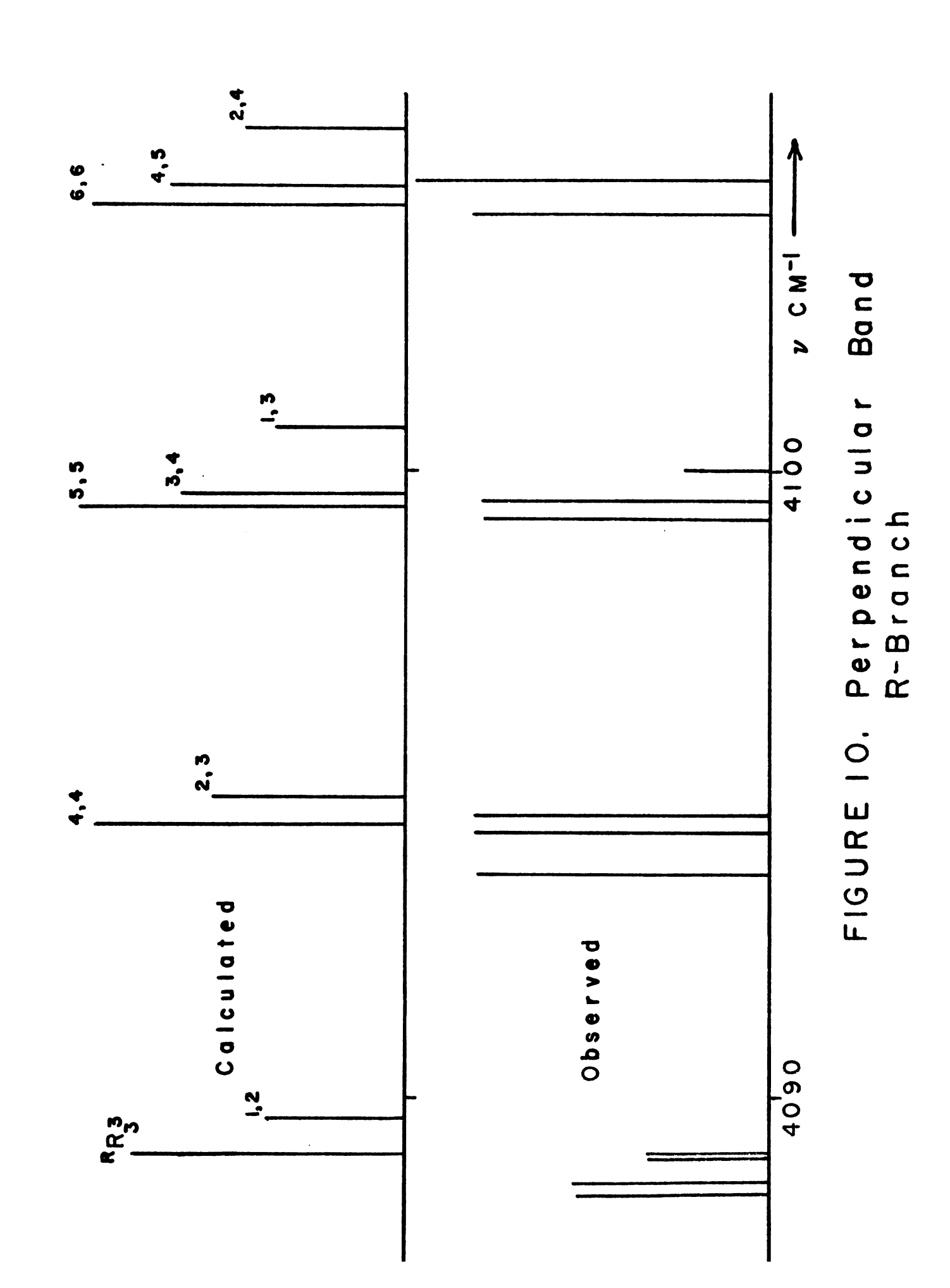
C' - C'' = -0.0707

B' - B" = -0.1956

 $v_o = 4063.741$







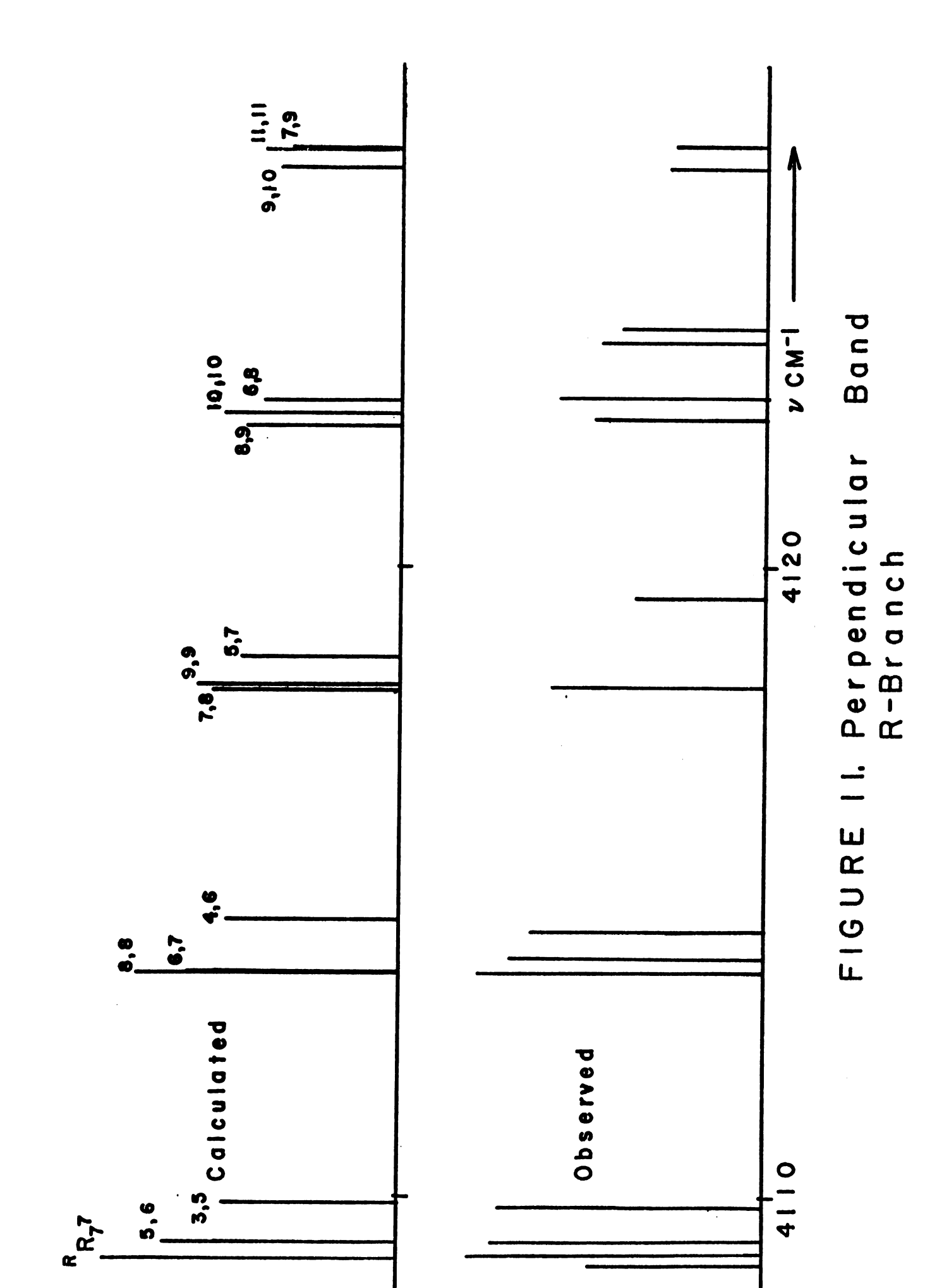


TABLE V

CALCULATED SYMMETRIC TOP

PERPENDICULAR BAND LINES

AND INTENSITIES

R-BRANCH

$^{R}R_{\kappa}(\kappa)$	I	$R_{K}(K+1)$	I	^R R _K (K + 2)	I
	-		-		
4072.75 4078.36 83.82 89.14 94.32 99.35 4104.24 9.00 13.61 18.08 22.40 26.58 30.63 34.53 38.28	5.70 .8.60 11.60 11.90 11.45 10.60 9.20 7.60 5.93 4.41 3.13 2.15 1.40 0.87 0.53	4089.72 94.80 99.73 4104.52 9.16 13.66 18.03 22.25 26.32	5.45 9.36 8.15 8.16 7.52 6.40 5.20 3.97 2.90	4100.70 5.39 9.93 14.32 18.58 22.70 26.67	4.96 5.78 5.95 5.40 4.60 3.66 2.75
41.90					
	4072.75 4078.36 83.82 89.14 94.32 99.35 4104.24 9.00 13.61 18.08 22.40 26.58 30.63 34.53	4072.75 5.70 4078.36 .8.60 83.82 11.60 89.14 11.90 94.32 11.45 99.35 10.60 4104.24 9.20 9.00 7.60 13.61 5.93 18.08 4.41 22.40 3.13 26.58 2.15 30.63 1.40 34.53 0.87 38.28 0.53	4072.75 5.70 4078.36 .8.60 4089.72 83.82 11.60 94.80 89.14 11.90 99.73 94.32 11.45 4104.52 99.35 10.60 9.16 4104.24 9.20 13.66 9.00 7.60 18.03 13.61 5.93 22.25 18.08 4.41 26.32 22.40 3.13 26.58 2.15 30.63 1.40 34.53 0.87 38.28 0.53	4072.75 5.70 5.45 4078.36 .8.60 4089.72 9.36 83.82 11.60 94.80 8.15 89.14 11.90 99.73 8.16 94.32 11.45 4104.52 7.52 99.35 10.60 9.16 6.40 4104.24 9.20 13.66 5.20 9.00 7.60 18.03 3.97 13.61 5.93 22.25 2.90 18.08 4.41 26.32 22.40 3.13 26.58 2.15 30.63 1.40 34.53 0.87 38.28 0.53	4072.75 5.70 5.45 4078.36 .8.60 4089.72 9.36 4100.70 83.82 11.60 94.80 8.15 5.39 89.14 11.90 99.73 8.16 9.93 94.32 11.45 4104.52 7.52 14.32 99.35 10.60 9.16 6.40 18.58 4104.24 9.20 13.66 5.20 22.70 9.00 7.60 18.03 3.97 26.67 13.61 5.93 22.25 2.90 18.08 4.41 26.32 22.40 3.13 26.58 2.15 30.63 1.40 34.53 0.87 38.28 0.53

TABLE VI

CALCULATED SYMMETRIC TOP

PERPENDICULAR BAND LINES

AND RELATIVE INTENSITIES

P-BRANCH

<u>к</u>	P _K (K) cm ⁻¹	I ——	$\frac{P_{K(K+1)}}{cm^{-1}}$	I	$\frac{P_{K(K+2)}}{cm^{-1}}$. I
1 2 3 4 5 6 7 8 9 10 11 12 13 14 15	4054.46 48.19 41.77 35.20 28.50 21.66 14.67 7.54 4000.26 3992.85 85.30 77.60 69.76 61.78 53.65	1.89 5.16 9.04 8.50 9.38 8.97 7.96 6.66 5.31 3.99 2.86 1.98 1.30 0.46	4041.54 34.87 28.06 21.10 14.01 6.78 3999.40	2.46 4.61 7.98 6.40 6.15 5.42 4.50	4028.22 21.16 13.96 6.62 3999.13	2.65 3.88 6.35 4.28 3.81

in Table VII together with the deviations. Further assignments did not seem warranted due to the lack of sufficient resolution.

The values obtained for B' and B" by the analysis (Table IV) are, as defined above, the average values

$$\bar{B}' = 1/2 (A' + B')$$
 and

$$\bar{B}^{"} = 1/2 (A^{"} + B^{"}).$$
 The

approximate values of A', B' and A'', B'' may be found (7) by making use of the relation

$$I_{C} \doteq I_{A} + I_{B} \tag{17}$$

or

$$1/G \doteq 1/A + 1/B \tag{18}$$

Substitution of \bar{B} into (17) solving simultaneously for A and B gives

$$A = \bar{B} + (\bar{B}^2 - 2BC)^{1/2}$$
 and

$$B = \bar{B} - (\bar{B}^2 - 2\bar{B}C)^{1/2}$$
.

Substitution of the values of \bar{B}' , \bar{B}'' , \bar{C}' , and \bar{C}'' from Table IV gives:

$$A' = 7.189 \text{ cm}^{-1}$$

B' = 4.961

C' ± 2.935

A" = 7.539

 $B^{**} = 5.001$

c" = 3.006

(In Table IV, the average sign $\ddot{\mathbf{B}}$ has been omitted.)

TABLE VII

ASSIGNMENT OF SOME OF OBSERVED TRANSITIONS
AND COMPARISON WITH CALCULATED LINES
FIRST LINES

R-BRANCH

		$R_{K}(k)$	
K	Observed cm	Calculated cm	Deviations cm
1 2 3 4 5 6 7 8 9	4089.15	4078.35 83.82 89.14 94.32 99.35 4104.24	01
7 8 9	4113,62 18.06	9.00 13.61 18.08	01 +.02
10 11 12	26.69 30.68	22.40 26.58 30.63	10 05
		P-BRANCH	
		P _K (K)	
K	Observed am	Calculated cm-1	Deviations cm
1 2 3 4 5		4054.46 48.19 41.77	
) 4 5	4035.23	35.20 28.50	03
6	4021.65	21.65	+.01

Conclusions

The process of obtaining the rotational constants of hydrogen telluride incorporated the results from a number of related but separate steps. In order to record its near infrared absorption spectrum, the gaseous hydrogen telluride had to be prepared, purified, introduced into the system and preserved long enough to obtain a spectrum.

The problem of preparation of hydrogen telluride was due to its instability and the low yield of the chemical process. The need for refrigeration of the multiple traverse cell resulted in its modification to allow for cooling.

The near infrared absorption spectrum of hydrogen telluride was obtained after learning to adjust and clean the multiple traverse cell and the spectrometer. The spectrum was then calibrated, using the Fabry-Perot fringes to extrapolate between argon emission lines.

The calibrated spectrum was analyzed as the perpendicular band of a rigid accidentally symmetric top. The spectrum was identified as being that of a Type-A band from the appearance of the bands, the degree of asymmetry and the assumed direction of change of dipole moment. It is believed that no Q branches were observed. Due to the large number of isotopes of hydrogen telluride, only a few lines could be assigned to specific transitions, but the calculated and observed spectra compare fairly well.

· · ·

BIBLIOGRAPHY

- 1. F. A. Jenkins and H. E. White, <u>Fundamentals of Optics</u>, McGraw-Hill Book Company, Inc., (1957)
- 2. M. I. T. Wavelength Tables, M. I. T. Spectroscopy Laboratory, The Technology Press M. I. T., New York, J. Wiley and Sons, Inc. (1939)
- 3. Humphreys and Powell,
- 4. J. U. White, J. Opt. Soc. Am. 32, 285 (1942)
- 5. N. I. Sax, <u>Handbook of Dangerous Materials</u>, New York, Reinhold Publishing Corporation, (1951)
- 6. K. Rossmann and H. H. Nielsen, Tech. Report, Ohio State University
- 7. Herzberg, Molecular Spectra and Molecular Structure, D. Van Nostrand Company, Inc., (1945)

ROOM USE ONLY

MICHIGAN STATE UNIVERSITY LIBRARIES
3 1293 03169 3892